
Article:
Ohkitani, K. (2011) Growth rate analysis of scalar gradients in generalized surface quasigeostrophic equations of ideal fluids. Physical Review E, 83 (3). 036317. ISSN 1539-3755

https://doi.org/10.1103/PhysRevE.83.036317

Growth rates analysis of scalar gradient in generalized surface quasi-geostrophic equations of ideal fluids

Koji Ohkitani

School of Mathematics and Statistics, University of Sheffield,

Hicks Building, Hounsfield Road, Sheffield S3 7RH, U.K.

(Dated: February 12, 2011)

Abstract

The growth rates of scalar gradients are studied numerically and analytically in a family of 2D incompressible fluid equations related to the surface quasi-geostrophic (SQG) equation. The active scalar is related to the stream function ψ by $\theta = (-\triangle)^{\alpha/2}\psi,\ (0 \leq \alpha \leq 2)$. A notable difference is observed in a comparison of the instantaneous growth rates in L^p and in L^∞ norms, depending on the stage of the time evolution. The crux is the phase-shift effect of singular integral operators, which displaces the peak location of the scalar gradient from that of the strain rate. On this basis, a method of detecting such a dislocation is proposed, in view of the importance of their coalescence needed for a possible blow-up. Moreover, it is found in the long-time evolution that a solution of the SQG equation (whose regularity is not known) is *less singular* than that of the 2D Euler equations (known to be regular) on the time interval covered by this computation. This consistently expands an earlier observation by A.J. Majda and E. Tabak, Phys. D 98, 515 (1996) in some detail. A 1D model problem is discussed for illustrating the present method and extensions to the 3D case is also are briefly discussed.

PACS numbers: Valid PACS appear here

I. INTRODUCTION

The regularity of incompressible fluid dynamics is an important but difficult problem in mathematical physics. We now understand at least qualitatively that the nonlinear terms of the fluid dynamical equations are subject to so-called nonlinearity depletion, associated with the emergence of spatially coherent structures. It is of importance to determine how effective this built-in mechanism can be in avoiding formation of a possible singularity. Normally nonlinearity depletion is thought to be related with geometric properties of fluid dynamical vector fields. We will consider a related, but a different effect in this paper.

Let us consider, for example, the vorticity equations in $\mathbb{R}^3$ in standard notations

$$\frac{D\boldsymbol{\omega}}{Dt} = \boldsymbol{S}[\boldsymbol{\omega}] \cdot \boldsymbol{\omega}, \tag{1}$$

where D/Dt denotes the Lagrangian time derivative. One important point is that the vorticity and the rate-of-strain should be coupled in a strong manner to develop a drastic self-amplification which can lead to finite-time blow-up. To this end, the local maximum of the vorticity and that of the rate-of-strain should be sufficiently closely placed to each other, because otherwise a strong coupling between them cannot take place. Obvious questions that arise are: how close should they be ?, or how may we decide that they are close enough ? In the case of 3D vorticity equations, the strain rate is given by a singular integral over the vorticity [1]

$$\boldsymbol{S}[\boldsymbol{\omega}](\boldsymbol{x}) = \frac{3}{8\pi}\mathrm{P.V.}\int_{\mathbb{R}^3} [\boldsymbol{y} \otimes \{\boldsymbol{y} \times \boldsymbol{\omega}(\boldsymbol{x}+\boldsymbol{y})\} + \{\boldsymbol{y} \times \boldsymbol{\omega}(\boldsymbol{x}+\boldsymbol{y})\} \otimes \boldsymbol{y}] \frac{d\boldsymbol{y}}{|\boldsymbol{y}|^5}, \tag{2}$$

where P.V. stands for a principal-value integral. See also [2] for an inversion of (2). The crux is that generally singular integral operators have the phase-shift effect, which may displace the peak locations of the vorticity and of the strain rate. As a typical example, we may recall that a Hilbert transform of $\sin x$ is $\cos x$, resulting in a phase-shift by $\pi/2$.

We propose a method of monitoring possible dislocation or coalescence of these peak positions. In this paper, we mainly consider a family of 2D incompressible systems, which includes the surface quasi-geostrophic (SQG) and the 2D Euler equations as special cases. The purpose of this paper is two-fold. The first one is to give a method of characterisation of dislocations in this case study. The second is to compare the SQG and Euler equations in some detail in the late stage of time evolution. We also study 1D model equations by

generalizing the Constantin-Lax-Majda (CLM, hereafter) equation [3] to see how the current method works.

Coalescence of peaks of the scalar gradient (a counterpart to the vorticity in the 3D Euler equations) and of the rate-of-strain is important for a possible blow-up. Such tests have often been adopted in the numerical experiments of the 3D Euler equations, e.g. in [4, 5]. It seems that there is some room for studying such an effect systematically.

The rest of this paper is constructed as follows. In Section II, a family of 2D incompressible fluid dynamics is reviewed, together with a summary of previous findings of the SQG equation. In Section III, numerical comparisons on the instantaneous growth rates of active scalar gradient are presented using various norms. In Section IV, an explanation of the comparison is given, together with the description of the long-time evolution. In Section V, similar considerations are given to model equations in one spatial dimension. Section VI is devoted to summary and discussion, with a brief discussion of the extension to the 3D case.

II. THE SQG RELATED FAMILY OF EQUATIONS

We consider a family of ideal incompressible fluid equations in two dimensions. The dynamics of an active scalar $\theta(\boldsymbol{x})$ is governed by the following equation

$$\frac{\partial \theta}{\partial t} + (\boldsymbol{u} \cdot \nabla)\theta = 0, \tag{3}$$

with smooth initial data $\theta(\boldsymbol{x}, t = 0) = \theta_0(\boldsymbol{x})$ and the velocity $\boldsymbol{u}$ given by

$$\boldsymbol{u} = \nabla^{\perp}\psi, \quad \Lambda^{\alpha}\psi = \theta \quad (0 \leq \alpha \leq 2). \tag{4}$$

Here $\nabla^{\perp} = (\partial_y, -\partial_x)$ denotes a skew gradient and $\Lambda \equiv (-\triangle)^{1/2}$ the Zygmund operator, which is defined by Fourier transform $\tilde{\Lambda} = |\boldsymbol{k}|$. The generalized system (3)-(4) has been considered in e.g.[6–9]. It reduces to the 2D Euler equations if $\alpha = 2$ and to the 2D SQG equation if $\alpha = 1$, and trivially to a steady state if $\alpha = 0$.

Mathematically, the best result of global existence available so far for the standard SQG equation (with $\alpha = 1$) is obtained with use of so-called hypo-viscosity introduced for interpolating inviscid and Newtonian viscous fluids. More precisely, for the hypo-viscous SQG equation

$$\frac{\partial \theta}{\partial t} + (\boldsymbol{u} \cdot \nabla)\theta = -\nu(-\triangle)^{\gamma}\theta \quad (0 \leq \gamma \leq 1), \tag{5}$$

it has been proved that if $\gamma \geq \frac{1}{2}$ we have no blow-up [10, 11]. See [13] for numerics of the hypo-viscous SQG equation in this context, As for the inviscid case, we only have local existence results and the mathematical problem of global regularity is markedly open; see [12] for weak solutions of the SQG equation.

The mathematical and computational study on the blow-up problem of the SQG equation was initiated by [14, 15]. In particular, for a flow which starts from the initial condition

$$\theta(\boldsymbol{x}) = \sin x \sin y + \cos y \tag{6}$$

an interpretation of finite-time blow-up was put forward using direct numerical simulations up to 1024^2 resolutions [14, 15]. An alternative interpretation of a rapid but regular, double-exponential growth in the scalar gradient of the form $\exp(\exp(t))$ was proposed, using up to 2048^2 resolutions [16]. This view has been subsequently supported by further numerical works such as [17, 18]. In this sense, numerical results suggest global regularity even for the ideal SQG equation, but it has turned out to be so difficult to prove it.

III. NUMERICAL RESULTS

A. Numerical method

We solve the SQG equation by a 2/3-dealiased standard pseudo-spectral method and a standard forth-order Runge-Kutta method for the initial data (6). The computations are done in double precision arithmetic. Just to give a general idea on the spatial resolutions for the inviscid case, we mention that previous inviscid computations could cover up to $t \approx 7$, while at the present resolution of 16384^2 we can cover up to $t \approx 9.5$ (Fig.1). In order to monitor numerical accuracy, we define the spectrum $Q(k)$ of the active scalar by

$$Q(k) = \frac{1}{2} \sum_{k \leq |\boldsymbol{k}| \leq k+1} |\tilde{\theta}(\boldsymbol{k})|^2. \tag{7}$$

In Fig.2 we show the spectra at $t = 9.0$ with two different resolutions $N = 8192$ and 16384. Both of them agree fairly well and we will basically use the data $N = 8192$ for analyses up to $t = 9.0$ in what follows.

B. Instantaneous growth rates

We consider the equation for an active scalar gradient $\boldsymbol{\chi} = \nabla^{\perp}\theta = \nabla \times \theta$,

$$\frac{D\boldsymbol{\chi}}{Dt} = \boldsymbol{\chi} \cdot \nabla \boldsymbol{u} \tag{8}$$

$$= -\boldsymbol{\chi} \cdot \boldsymbol{R}[\boldsymbol{\chi}], \tag{9}$$

where $\boldsymbol{R} = -\nabla\triangle^{-1}$ is the Riesz transform. In is well-known that presence or absence of blow-up can be monitored by a Beale-Kato-Majda-type criterion in terms of $|\boldsymbol{\chi}|$, that is, if $\int_0^T \sup_{\boldsymbol{x}} |\boldsymbol{\chi}(\boldsymbol{x}, t)| dt < \infty$, then the solution is regular up to $t = T$. It thus makes sense to study the growth of the magnitude of scalar gradient

$$\frac{D|\boldsymbol{\chi}|}{Dt} = a|\boldsymbol{\chi}|, \tag{10}$$

where the pointwise growth rate is defined by

$$a(\boldsymbol{x}, t) \equiv \frac{\boldsymbol{\chi} \cdot \nabla \boldsymbol{u} \cdot \boldsymbol{\chi}}{|\boldsymbol{\chi}|^2} = \frac{D}{Dt} \log |\boldsymbol{\chi}|. \tag{11}$$

In order to compare the growth of the scalar gradient among the equations in the whole generalized SQG family with different values of α, we may ask the following

Question: *Take a developed active scalar field, say, a snapshot of the SQG equation as an input. Compute growth rates in the L^p norm of the scalar gradient with various values of p, for a range of α ($0 \leq \alpha \leq 2$). Which α gives the maximum growth rate ?*

The results may and, in fact, do depend on the time chosen for the analysis as we will see below. We begin by considering a snapshot at $t = 5.0$. In Fig.3 we show the growth rate in terms of the L^2 norm as a function of α at $t = 5.0$. It should be noted that this growth rate generally increases with α. This appears to be rather counter-intuitive, because the 2D Euler equations ($\alpha = 2$) are known to be regular for all time, whereas the 2D SQG equation ($\alpha = 1$) has some room for a possible blow-up. Actually, it has been reported in [19] that the peak scalar gradient of the 2D Euler equations exceeds that of the SQG equation in the early stage of the time evolution. Then such a comparison deserves a closer investigation and should be clarified in more detail. In order to check the dependence on the choice of norms, in Fig.4 we plot a similar comparison with L^p ($p = 2, 4, \ldots, 10$) norms. Again, it is observed irrespective of p that the larger α we choose, the larger the growth rates of the scalar gradient takes.

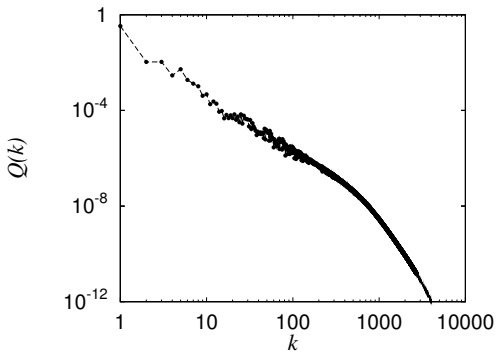

FIG. 1: Spectra of the active scalar at $t = 0.9$, with resolutions 8192^2 (circles) and 16384^2 (dashed line).

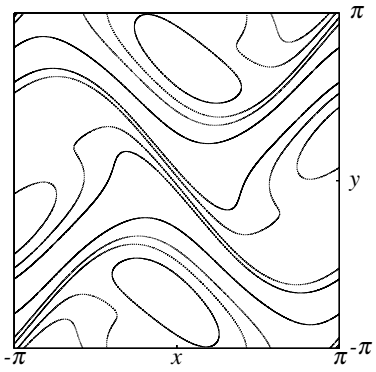

FIG. 2: Contours of the active scalar for the inviscid SQG ($\alpha = 1$) case at $t = 5.0$. Ten equally-spaced levels are used between the maximum and the minimum.

It is known that L^p norms with finite p are not strong enough to ensure the regularity of the solutions, that is, it can remain finite at a possible blow-up and its boundedness does not imply regularity. Stronger norms like the L^∞ norm (i.e. supremum), or, at least perhaps the BMO-norm are required to do that. In view of this, we repeat the the same kind of comparison using the L^∞ norm. In Fig.5 we show the growth rates measured in the L^∞ norm. It should be noted that with this norm the order is basically *reversed*, that is, it suggests that the SQG equation appears more singular than the 2D Euler equations, consistent with our intuition.

Our next task is to understand how this salient difference has come about qualitatively. First, it should be noted that the structure of the nonlinear terms in (8), the stretching of the scalar gradient is given by a product of the gradient and its singular integral transform (the Riesz transform). Second, we should recall that, generally speaking, singular integrals have the effect of phase shift. For example, in the case of the Hilbert transform H in 1D,

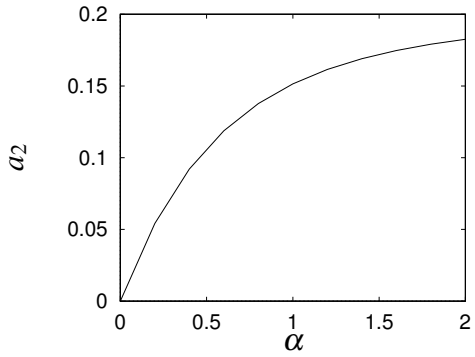

FIG. 3: Comparison of the growth rates a_2 of the active scalar gradient in the L^2 norm at $t = 5.0$ for the generalized SQG equations; SQG: $\alpha = 1$, 2D Euler: $\alpha = 2$.

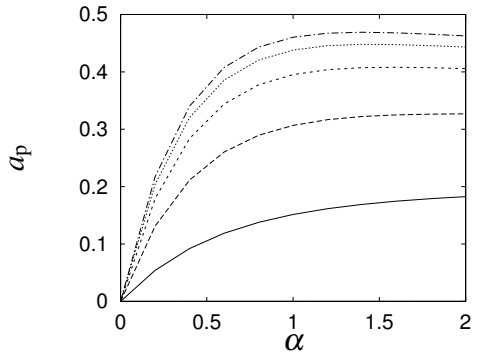

FIG. 4: Comparison of the growth rates a_p of the active scalar gradient in L^p norms at $t = 5.0$ for the generalized SQG equations: $p = 2, 4, 6, 8$ and 10 (solid, dashed, short-dashed, dotted and dash-dotted).

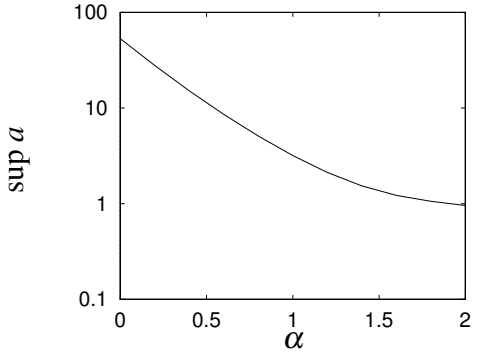

FIG. 5: Comparison of the growth rates sup a of the active scalar gradient in the L^∞ norm at $t = 5.0$ for the generalized SQG equations.

we have that

$$H\left[\frac{c}{x^2+c^2}\right] = \frac{x}{x^2+c^2}, \tag{12}$$

for any positive constant c. When c is small, the Hilbert transform maps a hump into a set of crest and a trough centered on the origin (see also Fig.17 below). This means that there is a displacement of the peaks of the transform in comparison with the original peak. Physically, we expect that in order to have a blow-up we need a strong coupling between the scalar gradient and the rate-of-strain in the quadratic nonlinear term, hence it is necessary their peaks must overlap.

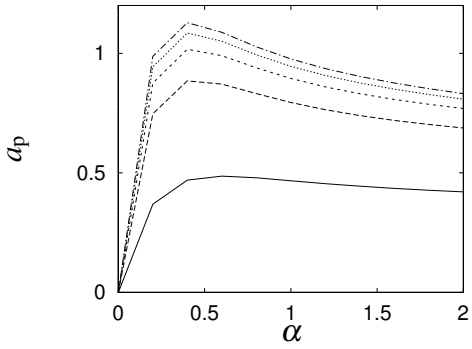

FIG. 6: Comparison of the growth rates a_p of the active scalar gradient in L^p norms at $t = 8.0$ for the generalized SQG equations: $p =$ $2, 4, 6, 8$ and 10 (solid, dashed, short-dashed, dotted and dash-dotted).

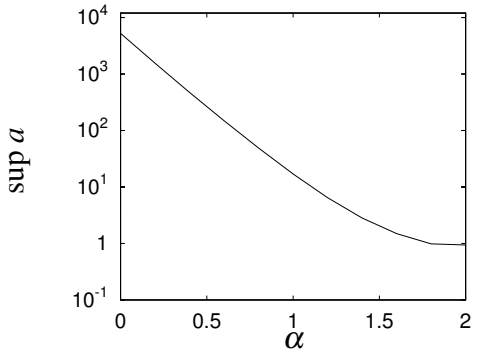

FIG. 7: Comparison of the growth rates sup a of the active scalar gradient in the L^∞ norm at $t = 8.0$ for the generalized SQG equations.

The above reasoning suggests that at a later stage when the fronts are developed even further, the trend in the growth rates as a function of α in L^p and in L^∞ norms may agree. In Fig.6 we show the growth rates using L^p norms at a later time $t = 8.0$. At this stage the growth rates a_p in L^p norms decrease with α, when $\alpha \geq 1$ for all p's, in a marked contrast to the case of $t = 5.0$. It is noted that for $p = 2$ the SQG equation has almost the same growth rates as the 2D Euler equations. Also, the growth rate in the L^∞ norm is again a decreasing function of α (Fig.7). Thus, in the late stage of evolution both kinds of growth rates, L^p and L^∞, show the same trend of decreasing with α.

IV. QUALITATIVE EXPLANATION

A. Two kinds of growth rates

In order to understand the above results of the numerical experiments, we take a closer look at the growth rate using various norms. If we define the L^p norms by $\|\boldsymbol{\chi}\|_{L^p} = \left(\int |\boldsymbol{\chi}|^p d\boldsymbol{x}\right)^{1/p}$, it satisfies

$$\frac{d}{dt}\|\boldsymbol{\chi}\|_{L^p} = \frac{\langle a|\boldsymbol{\chi}|^p\rangle}{\langle|\boldsymbol{\chi}|^p\rangle}\|\boldsymbol{\chi}\|_{L^p} = \underbrace{\langle a(\boldsymbol{x},t)|\hat{\boldsymbol{\chi}}|^p\rangle}_{=a_p(t)}\|\boldsymbol{\chi}\|_{L^p}, \tag{13}$$

where $\langle \quad \rangle = \int \quad \boldsymbol{dx}$ denotes a spatial integral and $\hat{\boldsymbol{\chi}} \equiv \boldsymbol{\chi}/\|\boldsymbol{\chi}\|_{L^p}$ the gradient normalized such that $\langle |\hat{\boldsymbol{\chi}}|^p \rangle = 1$. Here, we have introduced the averaged growth rate defined by

$$a_p(t) = \frac{d}{dt} \log \|\boldsymbol{\chi}\|_{L^p}. \tag{14}$$

It is readily checked that $a_p(t)$ can be written as a spatial average of the local growth rate $a(\boldsymbol{x}, t)$ weighted against the normalized scalar gradient

$$a_p(t) = \langle a(\boldsymbol{x}, t) |\hat{\boldsymbol{\chi}}|^p \rangle \,. \tag{15}$$

In the expression (15), if $|\boldsymbol{\chi}|$ is localized around $\boldsymbol{x} = \boldsymbol{x}_*$, we have $|\hat{\boldsymbol{\chi}}|^p \to \boldsymbol{\delta}(\boldsymbol{x} - \boldsymbol{x}_*)$ as $p \to \infty$, where δ denotes the Dirac delta function. We thus find

$$\lim_{p\to\infty} a_p(t) = a(\boldsymbol{x}_*, t), \quad \text{which, in general, } \neq \sup_{\boldsymbol{x}} a(\boldsymbol{x}, t). \tag{16}$$

(Note that in [15], $\sup_{\boldsymbol{x}} a(\boldsymbol{x}, t)$ is denoted by α^* and $a(\boldsymbol{x}_*, t)$ by $\bar{\alpha}$.) Hence it eventually picks up the strain rate at the peak location of $|\boldsymbol{\chi}|$. In other words, the 'sup' operation and the (logarithmic) time derivative do not commute in general

$$\sup_{\boldsymbol{x}} \frac{D}{Dt} \log |\boldsymbol{\chi}| = \sup_{\boldsymbol{x}} a(\boldsymbol{x}, t) \neq \lim_{p\to\infty} a_p(t) = \frac{d}{dt} \log \|\boldsymbol{\chi}\|_{L^\infty}. \tag{17}$$

The large p limit of the averaged growth rate picks up the growth at the peak of the scalar gradient, rather than the peak value of local growth rate.

Because coalescence of peaks of the rate-of-strain and the scalar gradient seems important, the above observation gives us a practical and operational method of monitoring possible dislocations. The working hypothesis is the following. Compare the growth rates in L^p and L^∞ norms as a function of some parameter (α in our case) and check the general trend is the same or not in L^p and in L^∞ norms as a function of α. If it is different it should be taken as a signature of dislocation of the peak scalar gradient from the peak rate-of-strain. That way the current method can be used to detect possible dislocations of the two maximum points.

B. Long-time evolution

The above results are based on the analysis at a particular, frozen instant of time. They do not tell us anything about the long-time evolution. Dynamically, we may carry out numerical simulations for a long-time as long as the flow is well-resolved.

We compare the long-time evolution of a (squared) norm of the scalar gradient

$$P(t) = \frac{1}{(2\pi)^2} \left\langle \frac{|\nabla\theta|^2}{2} \right\rangle \tag{18}$$

for different values of α in Fig.8. It should be noted that the norm of the 2D Euler equations ($\alpha = 2$) are larger than that of the 2D SQG equation ($\alpha = 1$), consistent with the analyses of the instantaneous growth rates in L^p made above both at $t = 5$ and at $t = 8$. Note that the case of $\alpha = 1.5$ comes somewhere in between. While mathematically this quantity $P(t)$ is not strong enough to control regularity of the solution, the comparison suggests regularity of the SQG equation rather than its finite-time blow-up.

In Fig.9, we show the maximum value of the scalar gradient. In this case the behaviors are a bit more complicated. The norm of the 2D Euler equations are greater than that of the SQG for most of the time, but toward the end of computation the solution to the SQG equation catches up with that of the 2D Euler equations. Again, this is consistent with the analyses on the growth rate in the L^∞ norm, where the SQG equation has a higher growth rate than 2D Euler equations. At the late stage, the case with $\alpha = 1.5$ again is placed in between most of the time and it also catches up and eventually supersedes that of the 2D Euler equations around $t = 7.0$.

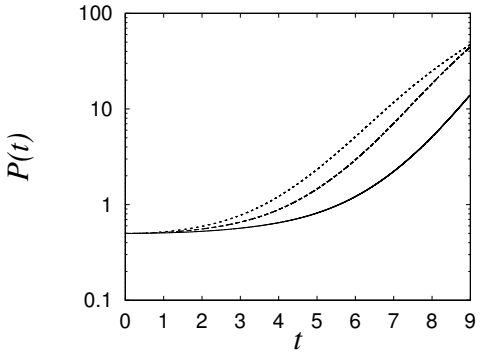

FIG. 8: Long-time evolution of $P(t)$ for the generalized SQG equations: $\alpha = 2$(dotted), 1.5(dashed) and 1(solid).

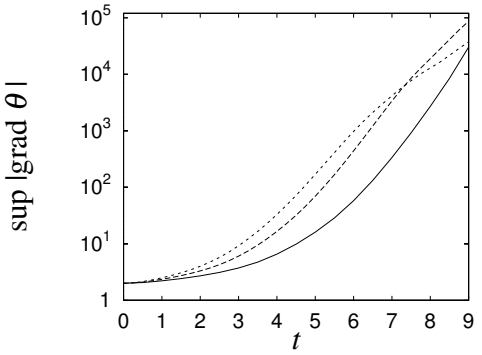

FIG. 9: Long-time evolution of sup $|\nabla\theta|$ for the generalized SQG equations: $\alpha = 2$(dotted), 1.5(dashed) and 1(solid).

In Figs.10-12 we compare the contour plots of the active scalar at $t = 8.0$ for $\alpha = 1, 1.5$ and 2. In all the three cases we find sharp gradient forming near the center of the domain. In order to compare the thickness of the sharp fronts we show cross sections of the contour at the center $(x, y) = (\pi, \pi)$ in Fig.13 ($t = 6.0$) and in Fig.14 ($t = 8.0$). Note that in order

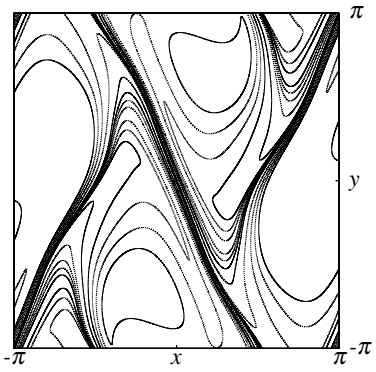

FIG. 10: Contours of θ for $\alpha = 2$ (the 2D Euler equations) at $t = 8.0$, plotted as in Fig.2.

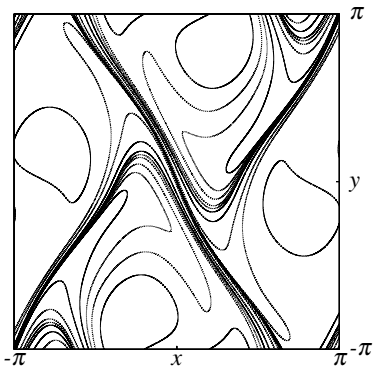

FIG. 11: Contours of θ for $\alpha = 1.5$ at $t = 8.0$, used. plotted as in Fig.2.

to compare the thickness properly we have sliced the sharp fronts orthogonally to them by using linear interpolations. It should be noted that at $t = 6$ the SQG equation has the widest layer and the 2D Euler equations the narrowest of all and that the case of $\alpha = 1.5$ comes just in between. At $t = 8$ the case $\alpha = 1.5$ has the sharpest front, but it is again the SQG equation ($\alpha = 1$) that has the widest layer. We conclude that the SQG equation has the mildest gradient of the active scalar out of the three cases in the time interval covered in the simulations.

V. 1D MODEL SYSTEM

In order to illustrate and see how the present method works, we consider here, the CLM model, a 1D model vorticity equation [3]

$$\frac{\partial \omega}{\partial t} = H(\omega)\omega, \tag{19}$$

with smooth initial data $\omega(x, t = 0) = \omega_0(x)$. Here

$$H(\omega) = \frac{1}{\pi}\text{P.V.}\int_{-\infty}^{\infty} \frac{\omega(y)}{x - y}\text{d}y \tag{20}$$

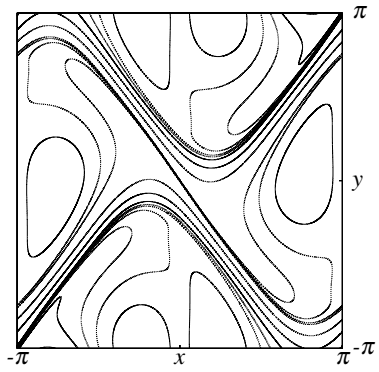

FIG. 12: Contours of θ for $\alpha = 1$ (the SQG equation) at $t = 8.0$, plotted as in Fig.2.

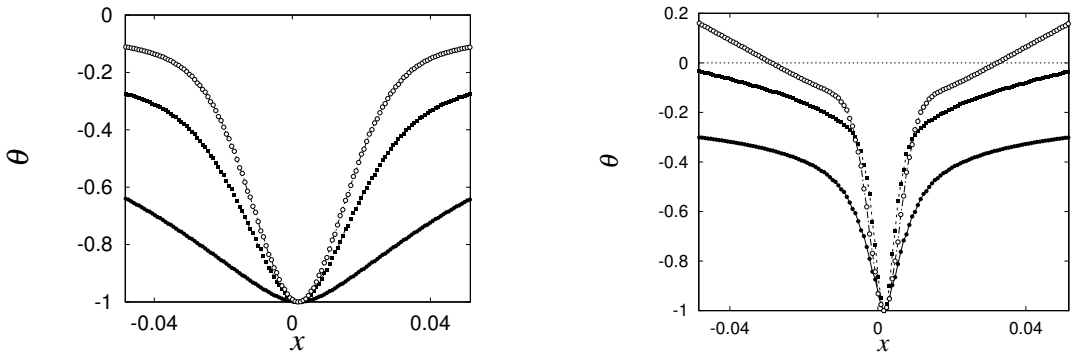

FIG. 13: Cross sections of $\theta(x, y)$ at $t = 6.0$, $\alpha = 2$:the Euler equations (open circles), $\alpha = 1.5$ (solid squares) and $\alpha = 1$:the SQG equation (solid circles).

FIG. 14: Cross sections of $\theta(x, y)$ at $t = 8.0$; $\alpha = 2$:the Euler equations (open circles), $\alpha = 1.5$ (solid squares) and $\alpha = 1$:the SQG equation (solid circles).

is the Hilbert transform. This model is exactly solvable, e.g. for the initial condition $\omega_0 = \cos x$, (for which $H[\omega_0] = \sin x$) under periodic boundary conditions, we have an exact solution of the form

$$\omega(x, t) = \frac{4 \cos x}{(2 - t \sin x)^2 + t^2 \cos^2 x}, \tag{21}$$

together with

$$H[\omega](x,t) = \frac{4\sin x - 2t}{(2 - t\sin x)^2 + t^2\cos^2 x}. \tag{22}$$

In order to apply the above method, we generalize the CLM model as

$$\frac{\partial \omega}{\partial t} = H_\alpha(\omega)\omega. \tag{23}$$

where we have introduced

$$H_\alpha \equiv -\partial_x \Lambda^{-\alpha}, \quad (0 \le \alpha \le 2) \tag{24}$$

with $\Lambda = (-\partial_x^2)^{1/2}$. The choice $\alpha = 1$ reduces to the original CLM model and the case $\alpha = 0$ corresponds to the Burgers equation $\omega_t + \omega\omega_x = 0$. See also [20, 21] for other related models in one dimension.

The pointwise growth rate in this case is given by

$$a(x,t) = H_\alpha[\omega] \tag{25}$$

and the averaged growth rate is defined by

$$a_p(t) = \langle a(x,t)|\hat{\omega}|^p\rangle = \frac{\langle H_\alpha[\omega]|\omega|^p\rangle}{\langle|\omega|^p\rangle}, \tag{26}$$

where $\hat{\omega}(x) \equiv \omega(x)/\|\omega\|_{L^p}$ denotes the normalized vorticity.

Except for the original case of $\alpha = 1$, it seems difficult to solve the system analytically. So we have solved numerically (23) by a 2/3 dealiased pseudo-spectral method under periodic conditions with $N = 4096$ grid points. Time marching was done by forth-order Runge-Kutta method with time increment $\Delta t = 1 \times 10^{-3}$. In Fig.15 we show growth rates measured in the L^p norm at rather early $t = 1.0$. (Remember it blows up at $t = 2.0$ for $\alpha = 1$.) It is monotonically increasing with respect to α. We next examine what happens if we measure the growth rate using the L^∞ norm. In Fig.16 we show the growth rate in the L^∞ norm. It shows that the growth rate decreases with α, in contrast to the growth rates in L^p. This contrast is similar to what we have found in the SQG family at the early stage.

In Fig.17, we show a snapshot of the vorticity and the strain rate at a late time $t = 1.8$, where we may confirm how the Hilbert transform maps a hump in the vorticity into a pair of a crest and a trough in the rate-of-strain near the center: $x = \pi$. It is readily checked by (21,22) that ω is peaked at $x = \tan^{-1}\frac{4t}{4-t^2}$ and $\|\omega\|_\infty = \frac{4}{4-t^2} \approx \frac{1}{2-t}$, as $t \to 2$, whereas $H[\omega]$ is peaked at $x = \pi/2$ and $\|H[\omega]\|_\infty = \frac{2}{2-t}$. Hence, an obvious inequality

$$\frac{d}{dt}\|\omega\|_\infty \le \|\omega\|_\infty \|H[\omega]\|_\infty \tag{27}$$

is an over-estimate, because of factor of 2 in the numerator in $\|H[\omega]\|_\infty$. Note that the peaks in ω and $H[\omega]$ are dislocated by $\approx 1 - t/2$ as $t \to 2$.

In the late stage at $t = 1.8$ we show in Fig.18 the growth rates measured in the L^p norms. The behavior is complicated in that it is not monotonic with respect to α, but as far as $\alpha \geq 1$ is concerned, it decreases with α. In Fig.19 we confirm that the growth rate in the L^∞ norm monotonically decreases with α. This agreement is similar to what we have in the late stage of the SQG family.

At the late stage of the time evolution, the general trend of the growth rates both for L^p and L^∞ norms are the same and indicates the peaks of the scalar gradient and the rate-of-strain are located sufficiently close to each other.

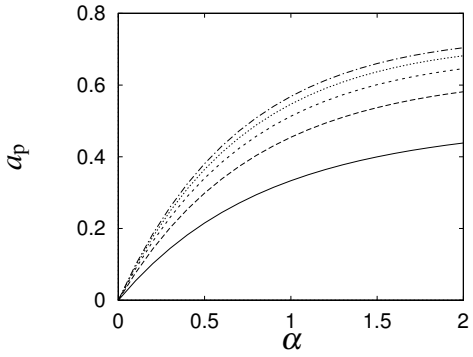

FIG. 15: Growth rates a_p in L^p norms at $t = 1.0$ for the generalized CLM models: $p =$ $2, 4, 6, 8$ and 10 (solid, dashed, short-dashed, dotted and dash-dotted).

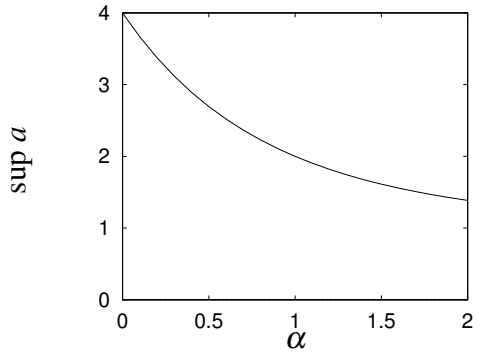

FIG. 16: Growth rates sup a in the L^∞ norm at $t = 1.0$ for the generalized CLM models.

VI. SUMMARY AND DISCUSSION

We have numerically studied the growth rates of scalar gradients in the generalized SQG equations using various norms and at the same time proposed a method for detecting dislocations of the peak strain and scalar gradient. This is based on the difference between the stretching rates measured in L^p and in L^∞ norms.

The current method rests on the principle that when we compare the growth rates in L^∞ and in L^p norms, the former is more sensitive to local dislocations than the latter. This can be used to monitor coalescence of local peaks in the scalar gradient and in the strain rate,

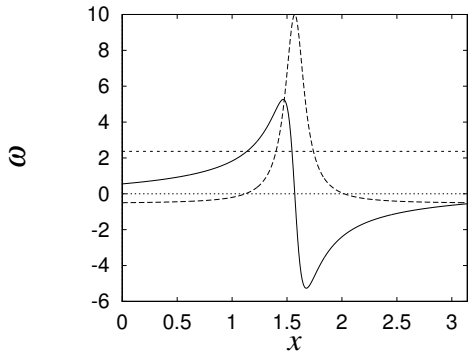

FIG. 17: Snapshots of the vorticity (solid) and rate-of-strain (dashed) of the CLM model at $t = 1.8$, $(t_* = 2)$. The horizontal dashed line denotes the averaged strain rate a_2.

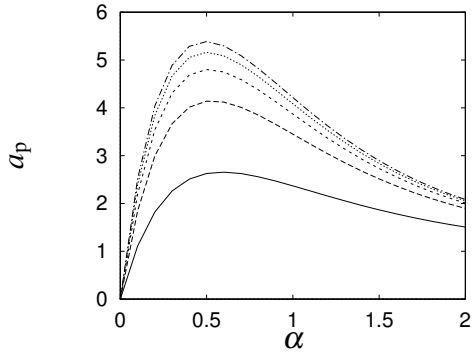

FIG. 18: Growth rates a_p in L^p norms at $t = 1.8$ for the generalized CLM models: $p =$ $2, 4, 6, 8$ and 10 (solid, dashed, short-dashed, dotted and dash-dotted).

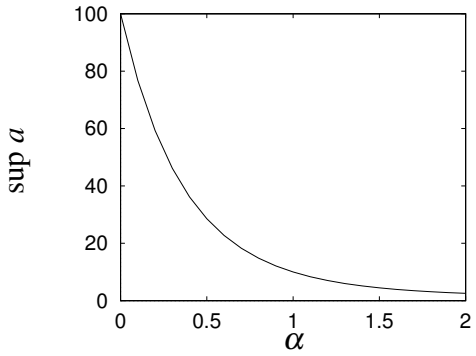

FIG. 19: Growth rates sup a in the L^∞ norm at $t = 1.8$ for the generalized CLM models.

which is necessary for a blow-up. We propose that by comparing the growth rates in L^p and L^∞ norms, we may detect such dislocations qualitatively. Note that growth may not be monotonic with respect to α; it depends on the time which exponent α gives the fastest growth at that time.

In the case of generalized CLM equations in one dimension, we have found the following. In the early stage the two kinds of the growth rates disagree in their trend but in the later stage they do agree. This is consistent with the presence of a finite-time blow-up in the model.

As long as the time interval covered by the present computations for current the initial data the scalar gradient of the SQG equation grows more slowly than that of the 2D Euler equations until the late stage. There is no sign of blow-up of the SQG equation in the time interval covered here, but it is catching up with the 2D Euler equations.

As in the case of 1D models, we have observed in the case of the generalized SQG family that late stage the trends in the growth rates disagree/agree in the early/late stage. That is, at $t = 5.0$ the growth rates in L^p norms increase with α, whereas the growth rate in the L^∞ norm decreases with α for $\alpha \geq 1$. Later at $t = 8.0$, both growth rates in L^p and L^∞ norms decrease with α for $\alpha \geq 1$. Toward the late stage covered in the present numerics, the flow behaves just like 1D models as far as this test is concerned. But it does not necessarily mean that the SQG equation is seeking a blow-up, because it may suffer from severe depletion of more geometric nature. It requires further work to settle this issue.

We may consider a similar comparison in three dimensions as well. In this case, we may generalize the 3D Euler equations as follows. That is, we replace the standard relationship for the vector potential $\boldsymbol{A}$, that is, $\triangle \boldsymbol{A} = -\boldsymbol{\omega}$ by

$$\Lambda^\alpha \boldsymbol{A} = \boldsymbol{W}, \quad (0 \leq \alpha \leq 2), \tag{28}$$

or

$$\boldsymbol{u} = \nabla \times \Lambda^{-\alpha} \boldsymbol{W}. \tag{29}$$

We then demand that

$$\frac{\partial \boldsymbol{W}}{\partial t} = \nabla \times (\boldsymbol{u} \times \boldsymbol{W}) \tag{30}$$

holds. Here $\alpha = 2$ reduces to the vorticity equations, and if $\alpha = 1$

$$\frac{\partial \boldsymbol{W}}{\partial t} = \nabla \times ((\nabla \times \Lambda^{-1} \boldsymbol{W}) \times \boldsymbol{W}), \tag{31}$$

which may be regarded as corresponding to the "SQG" case in 3D. It is of interest to study these generalized equations numerically.

Acknowledgments

Part of this work was presented at Institute for Mathematical Sciences workshop in May 2009 at Imperial College of London. The author has been benefited from discussions with the participants. It has been partially supported by an EPSRC grant EP/F009267/1. The

	$n=1$	$n=2$	$n=3$
$\alpha=0$	Burgers	steady	—
$\alpha=1$	"SQG"	SQG	"SQG"
$\alpha=2$	—	Euler	Euler

TABLE I: Parameters of generalized equations in other spatial dimensions, where "SQG" denotes a counterpart for the SQG equation in 2D.

author has been supported by Royal Society Wolfson Research Merit Award. The motivation has been augmented by attending a Workshop "The 3D Euler and 2D surface quasi-geostrophic equations" (March 30 to April 10, 2009) at American Institute of Mathematics.

[1] P. Constantin, SIAM Review **36**, 73 (1994).

[2] K. Ohkitani, Phys. Rev. E **50**, 5107 (1994).

[3] P. Constantin, P.D. Lax, and A. Majda, Commun. Pure Appl. Math. **38**, 715 (1985).

[4] R.M. Kerr, Phys. Fluids A **5**, 1746 (1993).

[5] T.Y. Hou and R. Li, J. Nonlinear Science **16**, 664 (2006).

[6] R.T. Pierrehumbert, I.M. Held and K.L. Swanson, Chaos, Solitons & Fractals **4**, 1111 (1994).

[7] I.M. Held, R.T. Pierrehumbert, S.T. Garner and K.L. Swanson, J. Fluid Mech. **282**, 1 (1995).

[8] J. Sukhatme and L.M. Smith, Phys. fluids **21**, 056603.1 (2009).

[9] C.V. Tran, D.G. Dritschel and R.K. Scott, Phys. Rev. E **81**, 016301-1 (2010).

[10] A. Kiselev, F. Nazarov and A. Volberg, Invent. Math. **167**, 445 (2007).

[11] L. Caffarelli and A. Vasseur, Annals. Math. **171**, 1903 (2010).

[12] P. Constantin, Physica D **237**, 1926 (2008).

[13] K. Ohkitani and T. Sakajo, Nonlinearity **23**, 3029 (2010).

[14] P. Constantin, A.J. Majda and E. Tabak, Nonlinearity **7**, 1495 (1994).

[15] P. Constantin, A.J. Majda and E. Tabak, Phys. Fluids **6**, 9 (1994).

[16] K. Ohkitani and M. Yamada, Phys. Fluids **9**, 876 (1997).

[17] P. Constantin, Q. Nie and N. Schörghofer, Phys. Lett. A **241**, 172 (1998).

[18] J. Deng, T.Y. Hou, R. Li and X. Yu, Methods Appl. Anal. bf 13, 180 (2006).

[19] A.J. Majda and E. Tabak, Phys. D **98**, 515 (1996).

[20] J. Qian, Phys. Fluids **27**, 1957 (1984).

[21] O. Zikanov, A. Thess and R. Grauer, Phys. Fluids **9**, 1362 (1997).